Comparison between field measurements and numerical simulation of steady-state solute transport in a heterogeneous soil profile

J. Vanderborght, D. Jacques, D. Mallants, P.-H. Tseng, J. Feyen

Hydrology and Earth System Sciences, 4, *853–871* (1997) © EGS

Hydrology & Earth System Sciences

Comparison between field measurements and numerical simulation of steady-state solute transport in a heterogeneous soil profile

J. Vanderborght*[1], D. Jacques[1], D. Mallants[1], P.-H. Tseng[2], and J. Feyen[1]

[1] Institute for Land and Water Management, KULeuven Vital Decosterstraat 102, B–3000 Leuven, Belgium
[2] Institute of Geophysics and Planetary Physics, UCR Riverside, CA 92521–0412, USA
* Corresponding author

Abstract

Field-scale solute dispersion is determined by water flow heterogeneity which results from spatial variability of soil hydraulic properties and soil moisture state. Measured variabilities of soil hydraulic properties are highly sensitive to the experimental method. Field-scale dispersion derived from leaching experiments in a macroporous loam soil was compared with field-scale dispersion obtained with numerical simulations in heterogeneous random fields. Four types of random fields of hydraulic properties having statistical properties derived from four different types of laboratory measurements were considered. Based on this comparison, the measurement method depicting heterogeneities of hydraulic properties most relevant to field-scale solute transport was identified. For unsaturated flow, the variability of the hydraulic conductivity characteristic measured on a small soil volume was the most relevant parameter. For saturated flow, simulated dispersion underestimated the measured dispersion and it was concluded that heterogeneity of macroscopic hydraulic properties could not represent solute flow heterogeneity under these flow conditions. Field-scale averaged solute concentrations depend both on the detection method and the averaging procedure. Flux-averaged concentrations (relevant to practical applications) differ from volume-averaged or resident concentrations (easy to measure), especially when water flow is more heterogeneous. Simulated flux and resident concentrations were subsequently used to test two simple one-dimensional transport models in predicting flux concentrations when they are calibrated on resident concentrations. In the first procedure, solute transport in a heterogeneous soil is represented by a 1-D convection-dispersion process. The second procedure was based on the relation between flux and resident concentrations for a stochastic-convective process. Better predictions of flux concentrations were obtained using the second procedure, especially when water flow and solute transport are very heterogeneous.

Introduction

Transport of inert solutes in a porous medium is driven by both advection and molecular diffusion. The advective transport is characterised by (i) the mean advective velocity which determines the average depth that a solute reaches after a certain time and (ii) the advection velocity fluctuations which contribute to the solute plume dispersion. When the advection velocities fluctuate over a scale much smaller than that over which solute concentrations are averaged and the scale of the transport process, i.e. the macroscopic scale, the effect of these fluctuations can be modelled as a Fickian, gradient-driven process (Dagan, 1989, p282) and the classical convection-dispersion equation (CDE) can be used to predict solute transport. In homogeneous soils, the scale of the velocity fluctuations is the pore-scale whereas in heterogeneous soils these fluctuations are persistent over a macroscopic scale. In general, soil heterogeneity results in a scale dependence of the solute dispersion which increases with increasing scale of the flow domain (Gelhar, 1993, p203,209). Two different types of heterogeneity causing macroscopic advection velocity fluctuations can be distinguished. The first type in structured soils comprises separate pore networks, macro- meso- and micro- in which solutes are advected with different velocities (White, 1985; Bouma, 1991). A second type is the spatial variability of macroscopic hydraulic properties (hydraulic conductivity, water retention characteristic). Macroscopic properties are averaged over a representative number of pores or a representative elementary volume (REV) which is sufficiently large so that the macroscopic properties when assigned to the centroid of the REV are continuous functions in space, yet sufficiently

small so that the spatial variability of the macroscopic properties is not averaged out (Bear, 1972, p19).

The observed heterogeneity of the macroscopic soil hydraulic properties depends, however, largely on (i) the size and the spatial scale of the soil sample on which the hydraulic properties are determined, and (ii) the measurement techniques used to evaluate the hydraulic parameters. A theoretical analysis by Indelman and Dagan (1993) revealed that the variability of the hydraulic conductivity of soil samples taken from a stationary isotropic random field decreases with increasing scale of the soil sample whereas the correlation scale increases with increasing sample scale. These theoretical findings are in agreement with the observed effect of the sample scale on the variability of the hydraulic conductivity (Lauren *et al.*, 1988; Mallants *et al.*, 1997a ; Mohanty *et al.*, 1994). The measurement method and simplifying assumptions in deriving the hydraulic properties from experimental data also have an impact on the hydraulic properties evaluated and their variance (van Wesenbeeck and Kachanoski, 1995; Mallants *et al.*, 1997b). When distinct pore networks are present (first-type heterogeneity), the hydraulic properties, especially the hydraulic conductivity, and their variance depend largely on the degree of saturation which in turn determines the pore networks where water and solutes are flowing. For instance, in structured soils, the saturated hydraulic conductivity and its variance increase drastically when the soil is completely saturated and larger pores between the structural elements contribute to flow. Given the large differences in variability of macroscopic soil hydraulic properties that are obtained using different measurement methods and the effect of this variability on field-scale solute dispersion, it is important to know which type of measurement method yields relevant information and can be used to predict field-scale solute dispersion.

Interpretation of solute concentrations depends on the detection mode. Two different detection methods yield distinct observations of solute concentrations, i.e., the flux-averaged and volume-averaged concentrations. Flux averaged concentrations are measured in the effluent whereas volume averaged or resident concentrations are observed in a soil volume. The flux concentration mode is the most relevant one to assess groundwater pollution since it is related directly to the solute mass flux. Kreft and Zuber (1978) and Parker and van Genuchten (1984) discussed the differences between flux and resident concentrations for convective-dispersive transport in a homogeneous porous medium. Solute flux concentrations in heterogeneous soils have been examined in terms of the stochastic properties of the hydraulic conductivity (Dagan *et al.*, 1992) and were shown to differ from resident concentrations in a similar way as in homogeneous soils (Shapiro and Cvetkovic, 1988). Since for the experimental characterisation of solute transport in a heterogeneous field resident solute concentrations were measured (e.g., Jacques *et al.*, 1997c) and given the practical relevance of flux concentrations, it is important to test procedures used to derive flux concentrations from resident concentration data.

The objectives of this study are twofold. The first is to test whether field-scale solute dispersion in a macroporous loam soil can be predicted from the spatial variability of macroscopic hydraulic properties and to identify which experimental method yields relevant information about the variability of macroscopic soil hydraulic properties. Therefore, field-scale solute dispersion derived from field-scale leaching experiments under both saturated and unsaturated conditions has been compared with field-scale dispersion derived from numerical transport simulations in generated heterogeneous fields having statistical moments of measured macroscopic soil hydraulic properties.

Secondly two procedures to derive flux averaged concentrations from resident concentrations in a heterogeneous soil profile are compared. One procedure is based on the relation between resident and flux concentrations for convective-dispersive transport in a homogeneous medium (Parker and van Genuchten, 1984); the second procedure is based on the stochastic-convective transport concept (Simmons, 1982; Jury and Roth, 1990).

Materials and Methods

CHARACTERISATION OF FIELD-SCALE SOLUTE TRANSPORT AND SOIL HYDRAULIC PROPERTY HETEROGENEITY

To characterise field-scale solute transport under unsaturated flow conditions in a macroporous loam soil (Udifluvent (Soil Survey Staff, 1992) or Eutric Regosol (FAO, 1990)), a leaching experiment was carried out at an experimental field plot in Bekkevoort (Belgium). The movement of a $CaCl_2$ solute spike (0.6 M $CaCl_2$, 0.0065 m infiltration depth; Jacques *et al.*, 1997a), applied to the soil surface and subsequently leached out under unsaturated conditions at a steady flow rate of 2.8 cm d^{-1}, was monitored along a 12m long transect using horizontally installed TDR probes (3 rod probes, probe length 0.5m, inter rod distance 0.046m) at 5 different depths (0.1, 0.3, 0.5, 0.7, and 0.9m) with 24 probes at each depth. Resident solute concentrations were derived from TDR-measured impedances using the procedure discussed by Heimovaara *et al.* (1995). From a nearby plot, 15 undisturbed 0.3m I.D. and 1.0m long undisturbed soil columns were taken. These columns were saturated with water and a pounded top boundary was maintained to assure saturated water flow. The movement of a $CaCl_2$ solute spike (0.007M $CaCl_2$, 0.72 m infiltration depth, Mallants, 1996) under saturated flow conditions within these columns was also monitored by horizontally installed TDR probes (2-rod probes, probe length 0.25 m, inter rod distance 0.025m) at 6 different depths (0.05, 0.15, 0.30, 0.45, 0.6 and 0.8m). For a detailed description of the unsaturated and saturated leaching experiments, the reader is referred to Jacques *et al.* (1997ab) and Mallants (1996), respectively.

To determine the hydraulic properties of the Bekkevoort experimental site, soil samples of various sizes were taken 1m apart along a transect of 30m. Water retention curves, $\theta(h)$ with θ (L^3 L^{-3}) the volumetric water content and h (L) the pressure head, were determined on 5.1cm long and 5cm diameter soil samples (Kopecky rings). Saturated conductivity, K_{sat} (L T^{-1}), was measured on both Kopecky rings and larger 20cm long and 20cm diameter samples (crust rings). Hydraulic conductivity curves, $K(h)$ and $K(\theta)$, were derived from local θ and h measurements at 6 different depths (0.05, 0.15, 0.30, 0.45, 0.6 and 0.8m) in 100cm long and 30cm diameter soil columns (large columns) during a drainage experiment. The pressure heads measured during the drainage experiments ranged from 0 to −100cm so that the $K(h)$ curve could be determined for this pressure head range only. This range is sufficiently large to characterise the pressure heads for the applied flow rate (2.8 cm d^{-1}). A detailed description of this data set is given by Mallants *et al.* (1997b).

Linear scaling was used to characterise the heterogeneity of the hydraulic properties (Warrick *et al.*, 1977; Hopmans, 1987, Vogel *et al.*, 1991). Two location dependent scaling factors α_h and α_K relate the local $h(\theta)$ and $K(\theta)$ characteristics to deterministic reference $h^*(\theta)$ and $K^*(\theta)$ characteristics:

$$h(\theta) = \alpha_h \, h^*(\theta) \tag{1}$$

$$K(\theta) = \alpha_K \, K^*(\theta) \tag{2}$$

The deterministic $\theta(h^*)$ was described by the van Genuchten (1980) water retention curve (WRC):

$$\theta(h^*) = \theta_r + \frac{\theta_s - \theta_r}{(1 + |\, ah^* \,|^n)^m} \qquad h^* < 0 \tag{3}$$

$$\theta(h^*) = \theta_s \qquad h^* < 0$$

where θ_s and θ_r (L^3 L^{-3}) denote the saturated and residual volumetric water content, respectively, and a (L^{-1}), n (–) and m (–) ($m = 1 - 1/n$) are shape factors. The parameters of the deterministic reference curve and the scaling factors α_h were determined from the water retention curves measured on the Kopecky rings using a least-squares optimisation procedure (Jacques *et al.*, 1997b). The linear scaling of the local WRCs to the reference curve implies: (i) that the measured WRCs are described by the same functional form as Eqn. (3), and (ii) that the variability of the measured WRCs is due to variance of the a parameter only and n, m, θ_s, and θ_r are deterministic. These assumptions were reasonably met for the soil considered (Mallants *et al.*, 1996).

The reference conductivity curve $K^*(h^*)$ is given by:

$$K^*(h^*) = \frac{K^*_{sat}\{1 - |\, ah^* \,|^{nm} [1 + |\, ah^* \,|^n]^{-m}\}^2}{[1 + |\, ah^* \,|^n]^{ml}} \qquad h^* < 0, \quad m = 1 - 1/n \tag{4}$$

$$K^*(h^*) = K^*_{sat} \qquad h^* \geq 0$$

where K^*_{sat} (L T^{-1}) is the reference saturated conductivity and ℓ is a pore connectivity parameter (Mualem, 1976; van Genuchten, 1980). When ℓ is fixed, the shape of the $K^*(h^*)$ curve is determined entirely by the shape of the $\theta(h^*)$ curve. As for the WRC, the linear scaling technique assumes that the shape factors n, m, and ℓ are deterministic. In Table 1, the parameters a, n, θ_s, θ_r, and ℓ for $\theta(h^*)$ and $K^*(h^*)$ are shown. The parameter values of the reference WRC were used for a, n, θ_s, and θ_r, and adjusted 1 by trial and error until a good match was obtained between the van Genuchten-Mualem $K^*(\theta)$ (Eqn. (4) with h^* substituted by θ according to Eqn. (3)) and the reference $K^*(\theta)$.

Table 1. Parameters of the van Genuchten WRC and the Mualem-van Genuchten conductivity characteristic for the reference $\theta(h^*)$ and $K^*(h^*)$ curves.

θ_s	θ_r	a (cm $^{-1}$)	n	K^*_{sat} (cm d $^{-1}$)	ℓ
0.4	0.001	0.0109	1.288	38	20

Heterogeneous fields of scaling factors, from which fields of hydraulic properties were derived using Eqns (1) and (2), were generated with geostatistical methods and water and solute movement were simulated in the generated heterogeneous fields. To generate these heterogeneous fields, the geostatistical parameters of the scaling factors must be defined.

Based on the data used to characterise the heterogeneity of soil hydraulic properties, four different cases were considered. For the first case, it has assumed that the pore space is geometrically similar at all locations in the field and the scale factor of the conductivity characteristic can be related to the scale factor of the WRC as (Miller and Miller, 1956) (similar field case):

$$\alpha_K = 1/\alpha_h^2 \tag{5}$$

Since α_h was lognormally distributed (Jacques *et al.*, 1997b), α_K is also lognormally distributed with:

$$\sigma^2 \ln(\alpha_K) = 4 \, \sigma^2 \ln(\alpha_h) \tag{6}$$

For the second case, scale factors α_K were derived from K_{sat} measurements on crust rings (crust ring case):

$$\alpha_K = K_{sat}/K^*_{sat} \tag{7}$$

$$K^*_{sat} = \exp(\langle \ln(K_{sat}) \rangle) \tag{8}$$

where $\langle \ln(K_{sat}) \rangle$ is the expected value or the ensemble average of the log transformed saturated conductivity.

For the third case, K_{sat} measurements on Kopecky rings were used to define the scale factors α_K (Kopecky ring

case) according to Eqns (7) and (8). K_{sat} measurements on the crust and Kopecky rings were lognormally distributed (Mallants *et al*, 1997a), so that α_K for the second and third cases are also lognormally distributed. From Eqn. (7), it follows that:

$$\sigma^2 \ln(\alpha_K) = \sigma^2 \ln(K_{sat}) \qquad (9)$$

For these three cases, K was measured only at saturation and ℓ in Eqn. (4) was chosen to be 0.5, a value suggested by Mualem (1976) when no data on $K(h)$ are available.

For the fourth case, the $K(h)$ characteristics determined from drainage experiments in the large columns were scaled to a reference $K^*(h^*)$ characteristic using a least-squares optimisation procedure (Mallants *et al.*, 1997b) and the α_K were determined according to Eqn. (2) (large column case). Again, α_K was lognormally distributed (Mallants *et al.*, 1997b). Since no correlation was found between α_h and α_K derived from measured K_{sat} or $K(h)$ characteristics (Jacques *et al.*, 1997b; Mallants *et al.*, 1997b), the scaling factors for the second to fourth cases were assumed to be uncorrelated.

Exponential correlograms characterised the spatial correlation, $\rho(x)$, of the log-transformed scaling factors:

$$\rho(x) = \exp\left[-\sqrt{\left(\frac{x_1}{\gamma_1}\right)^2 + \left(\frac{x_2}{\gamma_2}\right)^2}\right] \qquad (10)$$

with x (L) the spatial separation, γ_i (L) the correlation length with the indices 1 and 2 referring to the horizontal and vertical direction, respectively. The horizontal correlation length, γ_1, of $\ln(\alpha_h)$ and $\ln(\alpha_K)$ for the similar field case equals 1.5m and is based on experimental variograms of $\ln(\alpha_h)$ that are derived without exclusion of large-scale deterministic variation of $\ln(\alpha_h)$ along the transect (Jacques *et al.*, 1997b). No data were available to determine the vertical correlation length, γ_2, so it was set to 0.5m which is of the same order of magnitude as those reported in other studies (Jury, 1985; Russo and Bouton, 1992; Rockhold *et al.*, 1996). For the crust ring case, the horizontal correlation length of $\ln(\alpha_K)$ was also approximately 1.5m (Mallants *et al.*, 1997a) and the same correlation lengths were assumed for the crust ring and similar field cases. For the Kopecky ring and large column cases, the experimental horizontal variograms of $\ln(\alpha_K)$ showed a pure nugget effect (Mallants *et al.* 1996). When trends (large-scale deterministic variation) of $\ln(\alpha_h)$ along the transect were removed, the variograms of $\ln(\alpha_h)$ also showed a pure nugget effect (Jacques *et al.*, 1997b). For these cases, vertical and horizontal correlation lengths could not be derived from the experimental variograms and a 'guesstimate' about these correlation ranges had to be made. The correlation lengths for these cases were set to be 0.1m in both horizontal and vertical directions. This correlation scale is consistent with uncorrelated 1m (i.e. the minimal lag considered in the experimental variograms, Jacques *et al.*, 1997b) spaced observations. Since this correlation length is larger or of the same order of magnitude as the scale of the soil volume over which variables (water content, pressure heads, and water fluxes) are averaged by the measurement device or derivation technique, it is also consistent with the assumption that the derived hydraulic property variability represents the actual hydraulic property variability.

Table 2 summarises the variances of the log transformed scaling factors together with the horizontal and vertical correlation lengths of the four cases. Figure 1 shows the reference WRC $\theta(h^*)$ together with the WRCs which correspond to the 10% highest and lowest $\ln(\alpha_h)$ values and Figure 2 depicts similar curves for $K^*(h^*)$. For the second to fourth cases, α_K and α_h are not correlated and $K^*(h^*)$ curves corresponding to combinations of the 10% highest and lowest $\ln(\alpha_K)$ and $\ln(\alpha_h)$ are shown. For the fourth (large column) case, the shape of the $K^*(h^*)$ curve is different from that of the other cases owing to the deviating value of ℓ. The variability of $K(h)$ characteristics differs considerably between different cases (Table 2 and Fig. 2). The largest variability is observed for the smallest samples (Kopecky ring case) whereas the variability of $K(h)$ is the smallest when derived from the variability of the WRC (similar field case). For saturated conditions, when most of the water flow occurs in large pores between structural elements, the variability of the hydraulic conductivity, K_{sat}, is determined mainly by the variability of soil structure. This explains the discrepancy between $\sigma^2\ln(\alpha_K)$ derived from $\sigma^2\ln(\alpha_h)$ (similar field case) and $\sigma^2\ln(\alpha_K)$ derived from $\sigma^2\ln(K_{sat})$ (crust and Kopecky ring cases). Under unsaturated conditions, large pores between structural elements drained and the effect of soil structure variability on the hydraulic conductivity variability is smaller than that under saturated conditions; this explains why the $\sigma^2\ln(\alpha_K)$ is smaller for the large column case than for the Kopecky ring case. Small scale variations of soil structure explain the drastic decrease of $\sigma^2\ln(\alpha_K)$ with increasing averaging scale (Kopecky vs. crust ring cases), and the small correlation lengths of $\ln(\alpha_K)$ for the Kopecky ring and large column cases.

Table 2. Geostatistical parameters of the log-transformed scaling factors, α_h and α_K, used for the characterisation of the heterogeneity of soil hydraulic properties in the four cases (see text for explanation).

	$\sigma^2\ln(\alpha_h)$	$\sigma^2\ln(\alpha_K)$	γ_1 (m)	γ_2 (m)
similar field case	0.169	0.676	1.5	0.5
crust ring case	0.169	1.55	1.5	0.5
Kopecky ring case	0.169	3.6	0.1	0.1
large column case	0.169	2.55	0.1	0.1

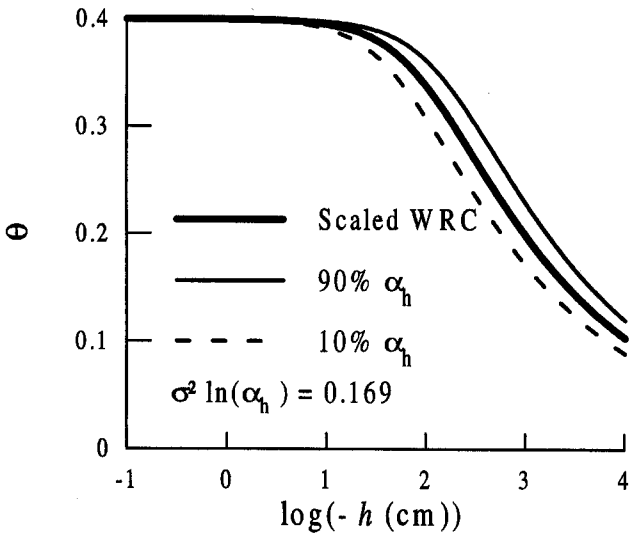

Fig. 1. *Reference water retention curve and water retention curves corresponding to the 10% highest and 10% lowest scaling factors* α_h. *(θ = volumetric water content; h = pressure head).*

GENERATION OF RANDOM FIELDS

A method based on the spectral representation theorem was used to generate random fields with a given variance and spatial covariance (Gutjahr *et al.*, 1995; Robin *et al.*, 1993). In the frequency domain, a (complex) random process is generated with properties defined by the spectral density function which is the Fourier transform of the spatial correlation function. The frequency domain random process is efficiently backtransformed to spatial domain random process by means of the fast Fourier transform, FFT. Thus, 2-D random fields of 512 by 512 nodes representing a vertical cross-section were generated. To avoid periodicity with periods equal to the dimensions of the domain resulting from discrete Fourier transformation (Robin *et al.*, 1993), subsections of 200 by 200 nodes of the larger fields were retained. Since an objective of this study is to compare simulated with measured field-scale solute transport and since the solute concentrations were measured to a depth of 0.9m, the depth of the random fields was restricted to 2m. To ensure that the simulated solute transport represents the transport in heterogeneous fields with specified statistical properties, i.e. to ensure ergodicity, the simulation fields should be sufficiently large. Several authors suggest using a field width of at least 20 correlation lengths to assure near-ergodic conditions (Cvetkovic *et al.*, 1992; Tompkins *et al.*, 1994). Therefore, the width of the simulation fields was chosen depending on the horizontal correlation scale. The dimensions of the simulation fields and the grid sizes are shown in Table 3. The horizontal grid size was small enough, i.e. more than 5 nodes per correlation length (Ababou *et al.*, 1989; Tompkins *et al.*, 1994) to ensure that small scale heterogeneity is not smoothed out during the numerical solution of the flow and transport equations which involve linear interpolation of the hydraulic properties in the grid elements. The vertical grid-size was determined by convergence and stability requirements for the numerical solutions of the flow and transport equations.

2-D SIMULATIONS OF WATER FLOW AND SOLUTE TRANSPORT

It is assumed that water flow in a rigid, variably saturated porous medium can be described by the Richards equation (Richards, 1931):

$$\frac{\delta\theta(h,x)}{\delta t} = \frac{\delta}{\delta x_i}\left[K(h,x)\left(\frac{\delta h}{\delta x_i} - \delta_{i2}\right)\right] \qquad (11)$$

where δ_{ij} is the Kronecker delta, and x_i (i =1, 2 for planar flow in a vertical cross-section) are the spatial co-ordinates with $x_2 = z$, the vertical co-ordinate which is positive downward. For a heterogeneous soil, both $\theta(h,x)$ and $K(h,x)$ vary with location, x. The mass flow of an inert dissolved solute in a heterogeneous soil is described by the convection-dispersion equation (CDE):

$$\theta(x)\frac{\delta C}{\delta t} = \frac{\delta}{\delta x_i}\left[\theta(x)D_{ij}(x)\frac{\delta C}{\delta x_j}\right] - \mathcal{J}_{wi}(x)\frac{\delta C}{\delta x_i} \qquad (12)$$

where C ($M\ L^{-3}$) is the concentration of the solute in the water phase, $\mathcal{J}_{wi}(x)$ ($L\ T^{-1}$) is the water flux in direction i and $D_{ij}(x)$ ($L^2\ T^{-1}$) is the ij entry of the dispersion coefficient tensor $\boldsymbol{D}(x)$. When neglecting molecular diffusion, $D_{ij}(x)$ is given by (Bear, 1972, p612):

$$\theta D_{ij}(x) = \lambda_T\,|\,\mathcal{J}_w(x)\,|\,\delta_{ij}\} + (\lambda_L - \lambda_T)\frac{\mathcal{J}_{wi}(x)\mathcal{J}_{wj}(x)}{|\,\mathcal{J}_w(x)\,|} \qquad (13)$$

where $|\mathcal{J}_w(x)|$ is the magnitude of the water flux vector $\mathcal{J}_w(x)$ and λ_L and λ_T (L) are the longitudinal and

Table 3. The scales of the simulation domains and grid sizes.

	Δx_1 (m)	Δx_2 (m)	width (m)	depth (m)
similar field and crust ring cases	0.15	0.01	29.85	1.99
Kopecky and large column cases	0.01	0.01	1.99	1.99

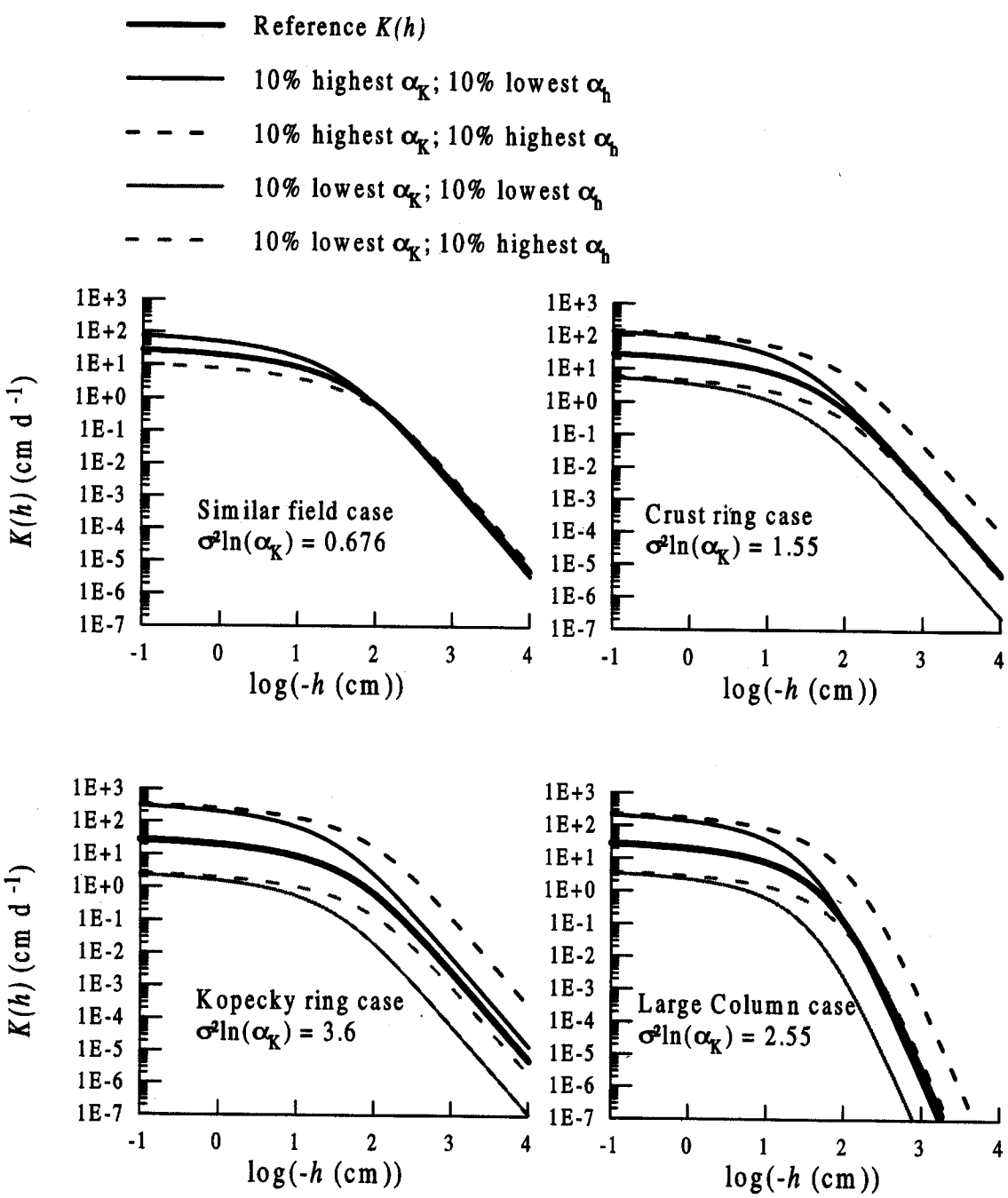

Fig. 2. *Reference conductivity curves and conductivity curves corresponding to the 10% highest and 10% lowest scaling factors α_K and α_h. (K = hydraulic conductivity; h = pressure head).*

transverse hydrodynamic dispersivities, respectively. For all cases, λ_L and λ_T were assumed to be 1 cm and 0.01 cm, respectively. This choice was based on the dispersivity of the field-scale measured solute plume close to the inlet surface which is determined mainly by pore-scale dispersivity (Toride and Leij, 1996).

Eqns (11) and (12) were solved numerically with the Galerkin finite element method by the SWMS_2D code (Šimůnek *et al.*, 1992). For the unsaturated flow simulations, a spatially uniform water flux top boundary, a free drainage bottom boundary condition and no flow lateral boundary conditions were implemented:

$$\mathcal{J}_{w2}(x, 0) = q;\ \mathcal{J}_{w2}(x, z_b) = K(\theta, x, z_b);\ \mathcal{J}_{w1}(x_l, z) = 0 \quad (14)$$

where $\mathcal{J}_{w1}$ and $\mathcal{J}_{w2}$ are the horizontal and vertical water flux densities, respectively, q = 2.8 cm d^{-1} is the constant uniform input water flux, z_b is the depth of the bottom boundary and x_ℓ is the horizontal location of the lateral boundary. For the saturated flow simulations, a zero head

top and bottom boundary condition and a no flow lateral boundary condition prevailed:

$$h(x, 0) = 0 \; ; \; h(x \; , \; z_b) = 0 \; ; \; \mathcal{J}_{w1}(x_\ell, \; z) = 0 \qquad (15)$$

The initial conditions, $h(x,z)$ at $t = 0$ were determined from the relation between the random processes of the hydraulic properties and pressure heads in the frequency domain (Harter and Yeh, 1993). After back transformation to the spatial domain, an approximation of the steady state pressure head distribution is obtained. Before solutes were applied to the soil surface, it was verified whether steady state conditions were obtained.

To solve the solute flow equation, an initially solute free soil profile, a solute flux top boundary, no flux lateral boundary and no vertical gradient lower boundary conditions were imposed:

$$C(x,z) = 0 \qquad t = 0 \qquad (16a)$$

$$-\theta D_{i2}(x,0)\frac{\delta C(x,0)}{\delta x_i} + \mathcal{J}_{w2}(x,0)C(x,0)\begin{cases} qC0 & 0 < t \le t0 \\ 0 & t0 \le t \end{cases} \qquad (16b)$$

$$\frac{\delta C(x_1 z)}{\delta x_1} = 0 \qquad (16c)$$

$$\frac{\delta C(x, z_b)}{\delta x_2} = 0 \qquad (16d)$$

where $C0$ is the concentration of the applied solution and $t0$ is the pulse duration. $t0$ was set to 0.02 d and $C0$ was chosen to make $C0$ $t0$ equal 1 day. When Eqn. (12) is solved for these boundary conditions, volume averaged or resident concentrations, $C^{\,r}$, are obtained. For many practical applications, the solute flux and flux averaged concentrations, $C^{\,f}$, at a certain depth are more relevant. For multi-dimensional transport, Sposito and Barry (1987) defined $C^{\,f}$ as the ratio of the projection of the solute mass flow in the direction of the water flow to the magnitude of the water flux. However, (i) since the direction of the water flux in soils is difficult to measure and (ii) the solute flux across a plane perpendicular to the mean water flow direction is of interest or is measured, $C^{\,f}$ was defined as the ratio of the vertical solute flow to the vertical water flow:

$$C^{\,f} = C^{\,r} - \frac{\theta(x)}{\mathcal{J}_{w2}(x)}\left[D_{i2}(x)\frac{\delta C^{\,r}}{\delta x_i}\right] \qquad (17)$$

CALCULATION OF BREAKTHROUGH CURVES (BTCS) OF FIELD AVERAGED FLUX AND RESIDENT CONCENTRATIONS AND DETERMINATION OF FIELD-SCALE DISPERSIVITY, λ_{EFF}, AND AVERAGE PARTICLE VELOCITY, V_{EFF}.

Time series of local concentrations at 15 selected depths (0.05, 0.1, 0.2, 0.3, 0.4, 0.5, 0.6, 0.7, 0.8, 0.9, 1.0, 1.2, 1.4, 1.6, and 1.8 m) were used to calculate a breakthrough curve (BTC) of field-scale averaged concentrations for each selected depth. A BTC of field-scale averaged resident concentrations along a transect at a depth z, $\hat{C}^{\,r}(t;z)$, was calculated by weighing the local resident concentrations along this transect by the local water content:

$$\hat{C}^{\,r}(t;z) = \frac{\sum_{i=1}^{200} \theta_i(z) C_i^{\,r}(t;z)}{200\langle\theta\rangle} \qquad (18)$$

$\theta_i(z)$ = water content at node i along the transect
$\langle\theta\rangle$ = average water content
$C_i^{\,r}(t;z)$ = resident concentration at node i along the transect

To calculate a BTC of field-scale averaged flux concentrations at a depth z, $\hat{C}^{\,f}(t;z)$, local flux concentrations along this transect were weighed by the local vertical water flux:

$$\hat{C}^{\,f}(t;z) = \frac{\sum_{i=1}^{200} \mathcal{J}_{w2i}(z) C_i^{\,f}(t;z)}{200\langle\mathcal{J}_{w2}\rangle} \qquad (19)$$

$\mathcal{J}_{w2i}(z)$ = vertical water flux at node i along the transect
$\langle\mathcal{J}_{w2}\rangle$ = average vertical water flux
$C_i^{\,f}(t;z)$ = flux concentration at node i along the transect

For the Kopecky ring and large column cases, solute transport was simulated in 4 realisations of the random field with dimensions given in Table 3. Field-scale averaged concentrations were calculated for each realisation using Eqns (18) and (19) and the arithmetic average of these concentrations was retained. This procedure was followed because the field-scale averaged concentrations differed somewhat from realisation to realisation.

The field-scale dispersivity, λ_{eff}, and field-scale average particle velocity, v_{eff}, are defined as the dispersivity and average particle velocity in an equivalent homogeneous soil column in which solute transport is described by a 1-D CDE. The 1-D CDE predictions of the BTC in the equivalent soil column then matches the field-scale BTC in the heterogeneous soil profile. For 1-D convective-dispersive transport in a homogeneous soil column, both resident and flux concentrations are described by (Parker and van Genuchten, 1984):

$$\frac{\delta \hat{C}}{\delta t} = D_{eff}\frac{\delta^2 \hat{C}}{\delta z^2} - v_{eff}\frac{\delta \hat{C}}{\delta z} \qquad (20)$$

with $D_{eff} = v_{eff}\,\lambda_{eff}$. When a third-type top boundary condition is applied to solve Eqn. (20), the solution yields a concentration in the resident domain:

$$\hat{C}^{\,r} - \frac{D_{eff}}{v_{eff}}\frac{\delta \hat{C}^{\,r}}{\delta z}\bigg|_{z=0} = \begin{cases} C0 & 0 < t \le t0 \\ 0 & t0 < t \end{cases} \qquad (21)$$

and a first type top-boundary condition yields the concentrations in the flux domain:

$$\hat{C}^{\,f}\Big|_{z=0} = \begin{cases} C0 & 0 < t \le t0 \\ 0 & t0 < t \end{cases} \qquad (22)$$

For each BTC of $\hat{C}^r$ and $\hat{C}^f$, D_{eff} and v_{eff} were determined by fitting the solution of the 1-D CDE equation using appropriate boundary conditions to the simulated BTCs in the random fields.

RELATION BETWEEN $\hat{C}^r$ AND $\hat{C}^f$

In general, for non-reactive solutes, $\hat{C}^f$ and $\hat{C}^r$ are related through a mass balance equation (Shapiro and Cvetkovic, 1988):

$$\hat{C}^r(z,t) = \hat{C}^r(z,0) - \frac{\langle \mathcal{J}_w \rangle}{\langle \theta \rangle} \frac{\delta}{\delta z} \int_0^t \hat{C}^f(z,t')\mathrm{d}t' \quad (23a)$$

$$\hat{C}^f(z,t) = \hat{C}^f(0,t) - \frac{\langle \theta \rangle}{\langle \mathcal{J}_w \rangle} \frac{\delta}{\delta z} \int_0^z \hat{C}^r(z',t)\mathrm{d}z' \quad (23b)$$

Derivation of $\hat{C}^f$ from $\hat{C}^r$ requires the evaluation of the depth integral in Eqn. (23b) which requires a detailed depth series of $\hat{C}^r$ measured with small time intervals. However, in practice, detailed time-series of $\hat{C}^r$ are usually available for only a limited number of observation depths or detailed depth series of $\hat{C}^r$ at only scattered observation times. When certain hypotheses on the transport process are made, the numerical evaluation of the integral in Eqn. (23b) can be circumvented. A first hypothesis is based on the assumption that field-scale solute flow can be described by a 1-D CDE process in an equivalent homogeneous soil column and that $\hat{C}^f$ and $\hat{C}^r$ are related as the flux and resident concentrations in the homogeneous soil column:

$$\hat{C}^r - \frac{D_{eff}}{v_{eff}} \frac{\delta \hat{C}^r}{\delta z} = \hat{C}^f \quad (24)$$

A second hypothesis assumes that solute transport can be conceptualised as a stochastic-convective process in which the velocity of a solute particle remains constant along its travel path (Simmons, 1982). For a stochastic-convective transport model, flux concentrations at two different depths z_1 and z_2 can be related as (Jury, 1982):

$$C^f(z_1;t) = \frac{z_2}{z_1} C^f\left(z_2; \frac{tz_2}{z_1}\right) \quad (25)$$

A stochastic-convective transport process is characterised by a linear increase of the effective dispersivity, D_{eff}, with depth (Simmons, 1982; Jury and Roth, 1990) which is analogous to the observed increase of D_{eff} close to the input surface in heterogeneous soils. As a result, the stochastic-convective transport concept is applicable for solute transport in heterogeneous soils close to the input surface (Tseng and Jury, 1994).

Using Eqn. (25) to evaluate field-scale flux averaged concentrations, $\hat{C}^f$, at different depths and times in the time integral of Eqn. (23a) yields the following relation between $\hat{C}^r$ and $\hat{C}^r$ for a stochastic-convective transport process (Jury and Roth, 1990):

$$\hat{C}^r(z,t) = C^r(z,0) + \frac{\langle \mathcal{J}_w \rangle}{\langle \theta \rangle} \frac{t}{z} \hat{C}^f(z,t) \quad (26)$$

Eqn. (26) can be used to derive $\hat{C}^f$ from $\hat{C}^r$ when field-scale solute transport can be described by a stochastic-convective process.

Results and Discussion

VARIABILITY OF WATER TRANSPORT

Figure 3 shows plots of the vertical component of the water flow vector, $\mathcal{J}_{w2}$, for the unsaturated flow simulations. Note that the horizontal scales used for the similar field and crust ring cases are different from those for the Kopecky ring and large column cases. In Table 4, mean (μ), variance (σ^2) and coefficient of variation ($CV\%$) of the water transport variables are given. Water flow is nearly homogeneous for the similar field case whereas for the other cases the uniform water flow at the inlet surface is clearly channelled in local 'stream tubes'. The higher $\sigma^2\ln(\alpha_K)$ and anisotropy ratio γ_2/γ_1 for the Kopecky ring and large column cases result in a higher CV of $\mathcal{J}_{w2}$ (Table 4 and Fig. 3) (Yeh *et al.*, 1985a and b; Russo, 1995a), and a larger magnitude of horizontal flow vector, $|\mathcal{J}_{w1}|$. However, the larger CV of $\mathcal{J}_{w2}$ for the saturated flow conditions is in contradiction to results based on a first-order perturbation analysis (Russo, 1995b) which is applicable only for $\sigma^2\ln(\alpha_K) < 1$ whereas $\sigma^2\ln(\alpha_K) = 3.6$ here. The shape and continuity of the stream tubes is determined by the spatial correlation of $\ln(\alpha_K)$. The vertical correlation

Table 4. Variability of the water transport parameters.

	$\lvert\mathcal{J}_{w1}\rvert$ (cm d^{-1})			$\mathcal{J}_{w2}$ (cm d^{-1})			θ			h (cm)		
	μ	σ^2	$CV\%$	μ	σ^2	$CV\%$	μ	σ^2	$CV\%$	μ	σ^2	$CV\%$
similar field case	0.14	0.015	90	2.8	0.06	9	0.375	0.00023	4	−35	51	20
crust ring case	0.63	0.9	151	2.8	1.06	37	0.375	0.00035	5	−41	1057	79
Kopecky ring case	1.25	3.46	149	2.8	12.38	125	0.375	0.00032	5	−41	485	57
large column case	1.03	2.03	138	2.8	8.23	102	0.387	0.00007	2	−20	93	48
saturated flow case (Kopecky rings)	15.6	645	162	37.9	2889	142	–	–	–	0	397	–

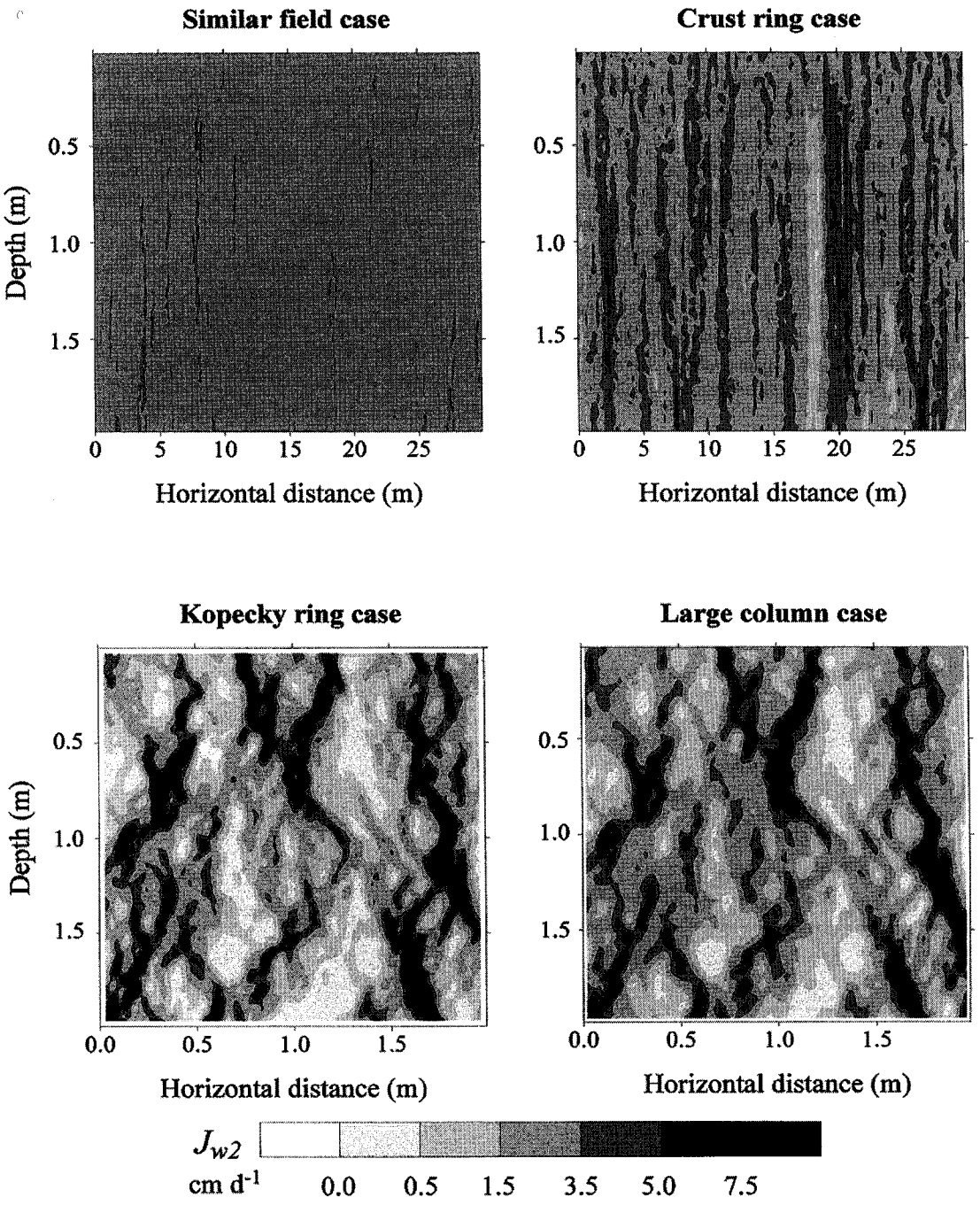

Fig. 3. *Simulated steady state vertical water fluxes, J_{w2}, for unsaturated flow conditions with a uniform water flux applied at the top boundary (infiltration rate = 2.8 cm d^{-1}).*

length of J_{w2} and J_{w1} is proportional to γ_2 and increases with decreasing anisotropy ratio γ_2/γ_1 (Russo, 1995a). This explains the nearly vertically continuous stream tubes along the simulation field for the crust ring case (γ_2 = 0.5m, γ_2/γ_1 = 0.333) whereas for the Kopecky ring and large column cases (γ_2 = 0.1m, γ_2/γ_1 = 1) stream tubes are more tortuous and are terminated or formed at various depths in the simulation field due to diverging or converging of stream lines.

The variabilities of h and of θ for the Kopecky ring and large column cases are lower than those for the crust ring case. This follows from the larger spatial correlation of $\ln(\alpha_K)$ for the crust ring case. According to Yeh *et al* (1985, a and b), these variances are proportional to $\sigma^2\ln(\alpha_k)\ \gamma_2^2$ and decrease with γ_2/γ_1. The lower absolute mean pressure head, $<|h|>$, for the large column case is due to a different $K^*(h^*)$ characteristic owing to a different ℓ parameter (cf. Fig. 2).

CONCENTRATION PROFILES

Figure 4 shows concentration profiles at 12.5 days after solute application. The solute concentration profile does not vary much along the transect indicating relatively homogeneous solute flow for the similar field case. For the other three cases, the concentration profiles vary considerably along the transect and reflect the water flow patterns shown in Fig. 3. Solute transport is mainly vertical for the crust ring case with unimodal depth profiles of concentrations at nearly all locations along the transect. For the Kopecky ring and large column cases, the concentration profiles are very irregular. Due to considerable horizontal solute flow, bi- or multi-modal depth profiles are observed at several locations along a transect. Owing to the small horizontal correlation of $\ln(\alpha_K)$ (γ_1 = 0.1m), solute concentrations vary over a small horizontal cross-section. This is in agreement with the conclusions drawn by Jacques *et al.* (1997c) who found that the major part of the solute flow heterogeneity observed at the field-scale is present within the 0.5m by 0.1m sampling area of a TDR probe.

BTCS OF $\hat{C}^r$ AND $\hat{C}^f$

In Fig. 5, $\hat{C}^r$ (Eqn. 18) and $\hat{C}^f$ (Eqn. 19) BTCs calculated at 1.0m below the input surface and normalised to *C0T0*, with *T0* the amount of water-filled pore volumes added during the application time *t0*, are plotted as a function of the number of water-filled pore volumes, $T = qt/z <\theta>$. The dispersion and the difference between BTCs for $\hat{C}^r$

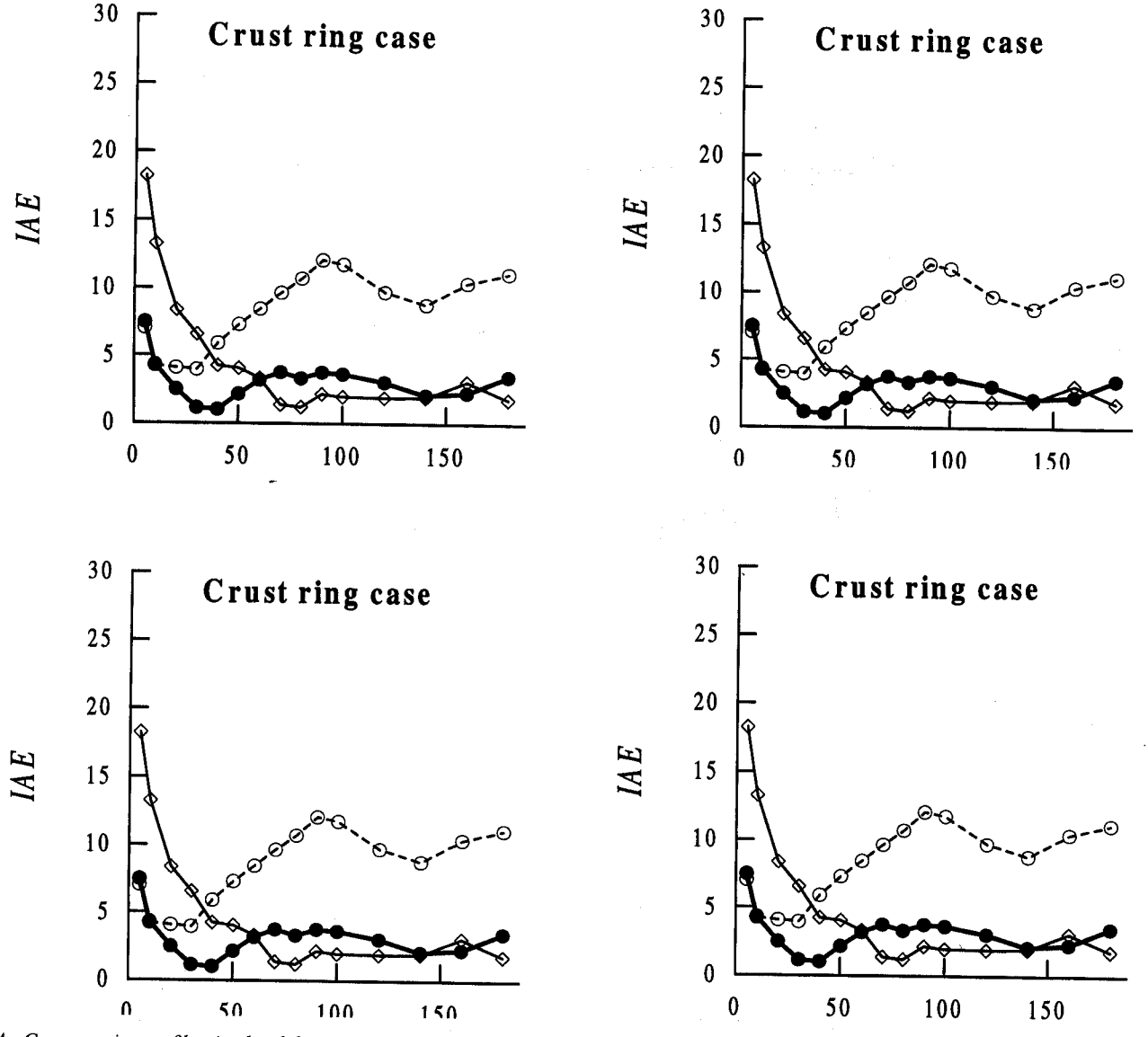

Fig. 4. *Concentration profiles simulated for steady state unsaturated flow (infiltration rate = 2.8 cm d^{-1}) 12.5 d after the start of solute application. Concentrations are normalised by C0t0, with C0 the concentration of the input solution and t0 the solute application time.*

and $\hat{C}^f$ increase with increasing heterogeneity of soil hydraulic properties and from unsaturated to saturated flow conditions (Fig. 5). The differences between $\hat{C}^f$ and $\hat{C}^r$ are analogous to the differences between resident and flux concentrations for homogeneous 1-D convective-dispersive transport when dispersive transport dominates (Parker and van Genuchten, 1984): i.e. higher peak concentrations and earlier arrival of the $\hat{C}^f$ BTCs. At the early stages of the breakthrough, $\hat{C}^f$ are larger than $\hat{C}^r$, which suggests that water fluxes are relatively high at locations where solutes leach rapidly.

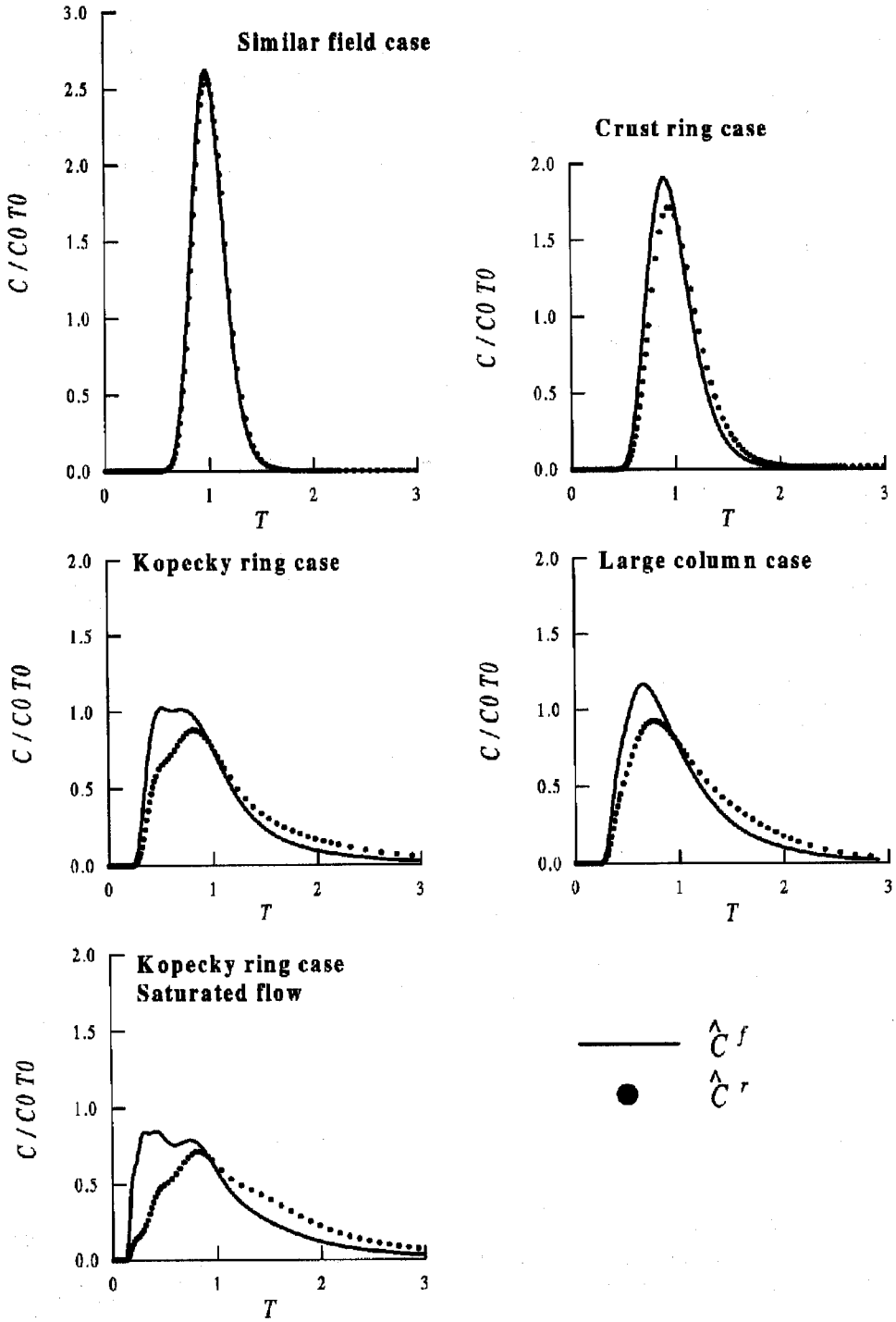

Fig. 5. *Breakthrough curves of simulated field-scale volume averaged concentrations, $\hat{C}^r$, and flux averaged concentrations, $\hat{C}^f$ at 1m depth. Concentrations are plotted versus the amount of water-filled pore volumes, $T = q\,t/\langle\theta\rangle\,z$, and are normalised with respect to C0T0, with C0 the concentration of the input solution and T0 the amount of pore volumes that was added during the solute application time.*

FIELD-SCALE EFFECTIVE DISPERSIVITY, λ_{EFF}, AND SOLUTE PARTICLE VELOCITY, V_{EFF}

Figure 6 shows the 'measured' field-scale dispersivity, λ_{eff}, derived from field-scale leaching experiments and the 'simulated' λ_{eff} which is derived from $\hat{C}^r$ and $\hat{C}^f$ BTCs simulated in random fields. For the unsaturated flow leaching experiment, two values of measured λ_{eff} derived from the same concentration data using different methods (Jacques *et al.*, 1997a) are given. The measured λ_{eff} are much larger for saturated than for unsaturated flow conditions and for both conditions, the measured λ_{eff} increase with increasing depth consistent with a stochastic-convective transport process.

Depending on which experimental method is used to characterise the heterogeneity of soil hydraulic properties, different simulated λ_{eff} are obtained. At comparable depths, the simulated λ_{eff} increases with increasing heterogeneity of the simulated $\mathcal{J}_{w2}$ (Table 4) which in turn increases with increasing heterogeneity of the hydraulic conductivity, $\sigma^2\ln(\alpha_K)$ (Table 2), and from unsaturated to saturated flow conditions (Table 4, Kopecky ring case). Except for the similar field case, the simulated λ_{eff} increases considerably with increasing depth. For the Kopecky ring and large column cases, the rate of increase diminishes at greater depths indicating mixing between fast and slow moving solutes owing to piece-wise continuous stream tubes and horizontal water flow (Fig. 3) which result from the small vertical correlation length of $\ln(\alpha_K)$, γ_2 (Table 2). However, simulated solute transport preserves the stochastic-convective nature relatively well for the range of depths at which solute transport was observed, despite the relatively small γ_2 value (0.1 m). Deeper in the soil profile, the stochastic-convective process shifts gradually towards a convective-dispersive process characterised by a constant λ_{eff}. For the crust ring case, due to a larger vertical correlation length of $\ln(\alpha_K)$ (Table 2) resulting in vertical continuous stream tubes (Fig. 3), simulated transport can be conceptualised as a stochastic-convective process for all depths in the simulation domain.

In this paragraph, λ_{eff} derived from leaching experiments and from transport simulations are compared to identify a measurement technique which provides relevant information about the hydraulic property heterogeneity for the prediction of field-scale solute transport. First, results for unsaturated and subsequently for saturated conditions are discussed.

For the similar field case, the simulated λ_{eff} differ only slightly from the pore-scale dispersivity (λ_T = 1 cm) and underestimate the measured λ_{eff} considerably owing to an underestimation of $\sigma^2\ln(\alpha_K)$ which was derived from the variability of the WRC or pore size distribution using the similar medium concept. Therefore, the variability of the pore size distribution is not a relevant parameter but conductivity measurements are required to determine the heterogeneity of macroscopic hydraulic properties.

The simulated λ_{eff} also underestimate the measured ones for the crust ring case and $\sigma^2\ln(\alpha_K)$ derived from conductivity measurements on the crust rings is too small. The heterogeneity of water flow and solute transport within the crust rings, which is averaged out, contributes significantly to the field-scale solute dispersion and conductivities should be measured on sufficiently small soil volumes to identify the soil heterogeneity properly.

For the Kopecky ring case, especially at shallower depths, the simulated λ_{eff} overestimates the measured λ_{eff}, indicating that water flow heterogeneity and $\sigma^2\ln(\alpha_K)$ are overestimated. Due to the soil macroporosity, the water flow heterogeneity is much larger under saturated than unsaturated conditions and the variability of the hydraulic conductivity for unsaturated flow is overestimated when based on K_{sat} measurements of small soil samples. For the large column case, using the variability of the $K(h)$ characteristics properly reflects the variability of the hydraulic conductivity for unsaturated flow conditions; hence, the best agreement between measured and simulated λ_{eff} is obtained. However, at shallower depths, the simulated λ_{eff} still overestimate the measured λ_{eff} indicating that water flow heterogeneity close to the spatially uniform water flow inlet surface is not well represented. It should be noted that the heterogeneity which gave the best results ($\sigma^2\ln(\alpha_k)$ = 2.5) is relatively large when compared to heterogeneities considered in first-order perturbation analyses of solute and water transport in heterogeneous soils and aquifers ($\sigma^2\ln(\alpha_k) < 1$). The field-scale dispersivities that are observed and simulated for this relatively large heterogeneity are, however, of the same order of magnitude (10^{-1} m), as those measured in other field-scale experiments (Beven *et al.*, 1993).

For saturated flow conditions, the simulated λ_{eff} underestimate the measured λ_{eff} considerably even if $\sigma^2\ln(\alpha_K)$ derived from K_{sat} measurements on Kopecky rings, which exhibit the largest variability, is used. Therefore, water flow and solute transport heterogeneities at a scale smaller than the size of a soil sample, such as flow and transport in different pore networks (first-type heterogeneity), is important under saturated flow conditions. Flow and transport in different flow domains can be modelled using a set of coupled flow and transport equations which describe flow and transport in each flow domain and the water and solute exchange between the pore domains (e.g. Jarvis *et al.*, 1991; Gerke and van Genuchten, 1993). Therefore, the hydraulic properties of each pore domain and the interaction coefficients should be determined. Since macro-pores are only filled with water and activated for transport of solutes under saturated conditions, water flow and solute transport under unsaturated flow conditions can be described by models that consider flow in only one pore network (Eqns (11) and (12)) and flow heterogeneities can be derived from the spatial variabiltity of macroscopic hydraulic properties.

From Fig. 6 it is also clear that λ_{eff} derived from $\hat{C}^r$

BTCs are larger than λ_{eff} derived from $\hat{C}^{f}$ BTCs. Figure 7 shows v_{eff} derived from $\hat{C}^{r}$ and $\hat{C}^{f}$ together with the field-scale mean solute velocity, $<J_{w2}>/<\theta>$, of a piston flow model. v_{eff} also depends on the concentration mode and is smaller when derived from $\hat{C}^{r}$ BTCs. The relative differences of λ_{eff} and v_{eff} derived from the two concentration modes are larger for larger $\sigma^2\ln(\alpha_K)$ when the transport process can be conceptualised as a stochastic-convective process. Time series of $\hat{C}^{f}$ represent solute travel time probability density functions (Simmons, 1982; Jury and Roth, 1990; Dagan *et al.*, 1992) and λ_{eff} and v_{eff} derived from are of more physical relevance and can be

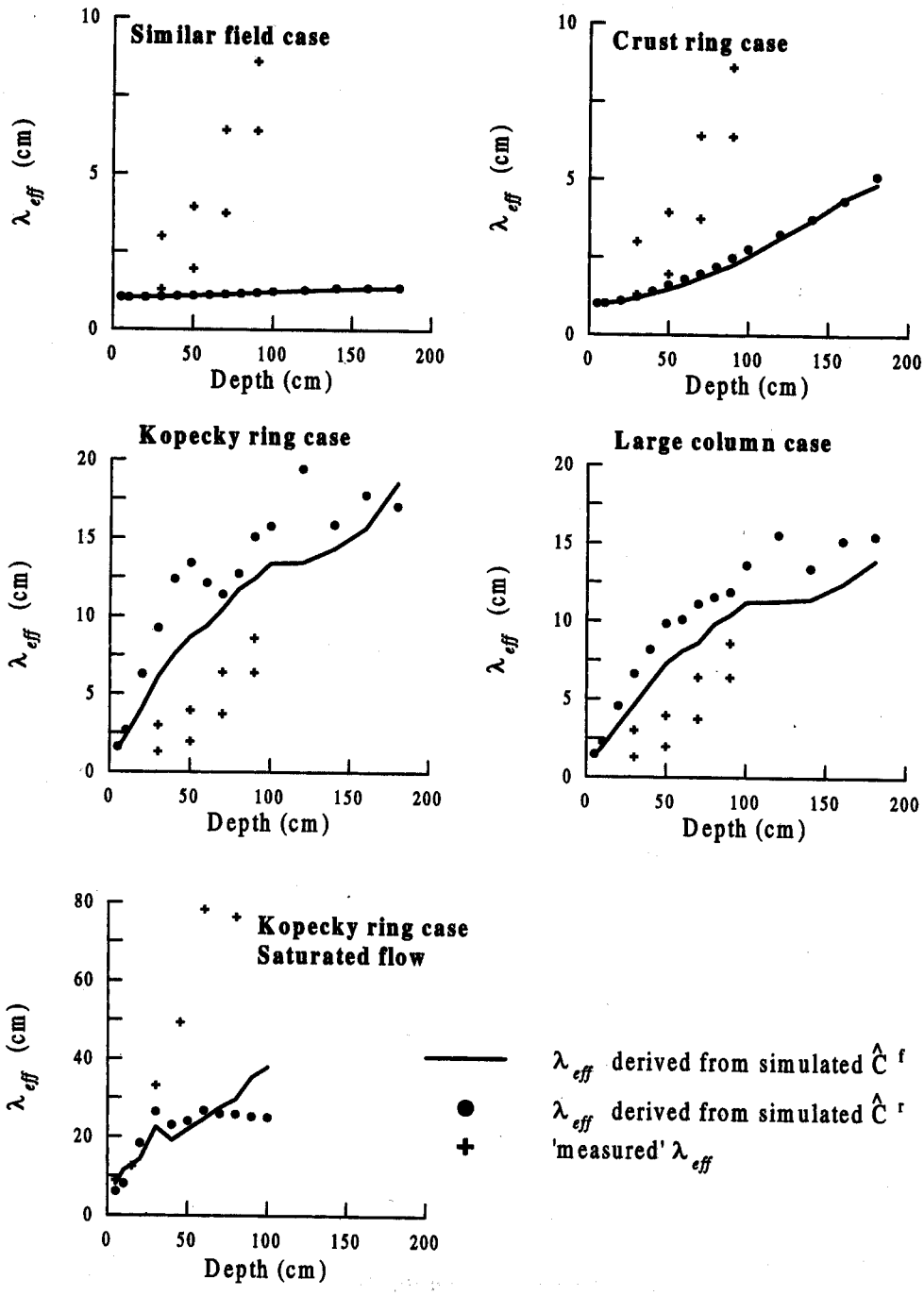

Fig. 6. *Effective dispersivities, λ_{eff}, derived from BTCs of measured field-scale averaged solute concentrations and from simulated BTCs of both volume and flux averaged concentrations.*

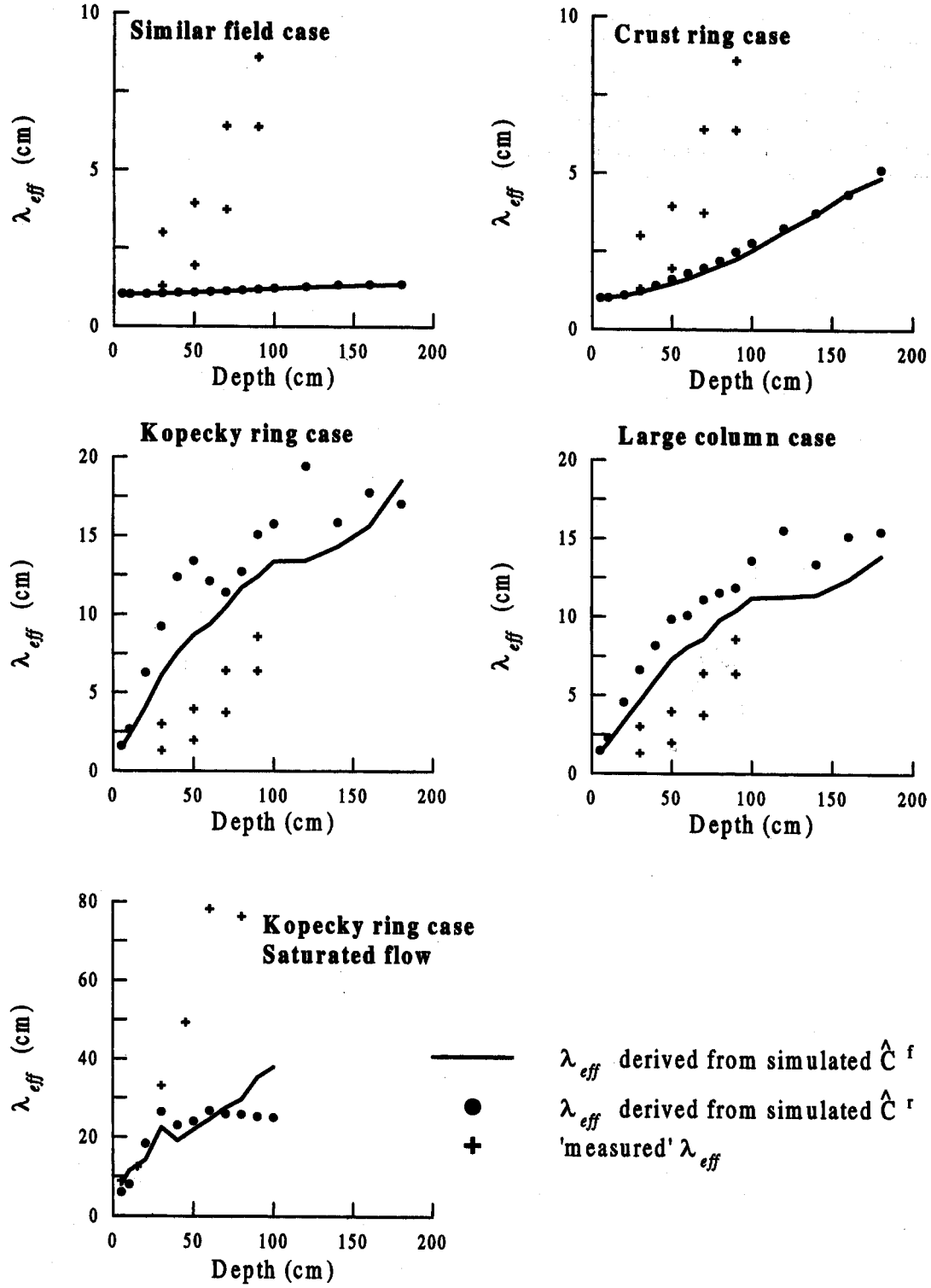

Fig. 7. *Effective average particle velocities, v_{eff}, derived from simulated BTCs of field-scale volume averaged and flux averaged concentrations and the piston flow particle velocities, $v = \langle J_{w2}\rangle / \langle\theta\rangle$.*

compared to $\langle J_{w2}\rangle / \langle\theta\rangle$. This comparison suggests that for larger $\sigma^2\ln(\alpha_K)$ and stochastic-convective transport, solutes are leached out faster than under piston-flow conditions which indicates 'preferential' flow. However, when v_{eff} is calculated from the time moments of $\hat{C}^f$ BTCs (Jury and Sposito, 1985), v_{eff} is nearly identical to $\langle J_{w2}\rangle / \langle\theta\rangle$ (results not shown). Therefore, the larger v_{eff} obtained from fitting the 1-D CDE to the simulated BTCs are due to a lack-of-fit. Simulated BTCs are more skewed than the fitted ones which underestimate simulated solute concen-

trations at later times. These results imply that when resident concentrations are observed in a field-scale leaching experiment with very heterogeneous and stochastic-onvective solute transport, the average solute travel time and solute dispersivity are overestimated if an effective 1-D CDE model is used to interpret the data. If flux averaged concentrations are observed, the average solute travel time is underestimated due to a lack-of-fit between the observed and the 1-D CDE predicted BTC.

DERIVATION OF $\hat{C}^f$ BTCS FROM $\hat{C}^r$ BTCS

Figure 8 shows simulated $\hat{C}^f$ BTCs together with $\hat{C}^f$ BTCs predicted by the 1-D CDE using v_{eff} and λ_{eff} which are calibrated to simulated $\hat{C}^r$ BTCs and $\hat{C}^f$ BTCs that are derived from simulated $\hat{C}^r$ BTCs using Eqn. (26). As could be expected based on the differences between λ_{eff} and v_{eff} derived from $\hat{C}^f$ and from $\hat{C}^r$ BTCs, the predictions of $\hat{C}^f$ BTCs by the 1-D CDE calibrated on $\hat{C}^r$ BTCs

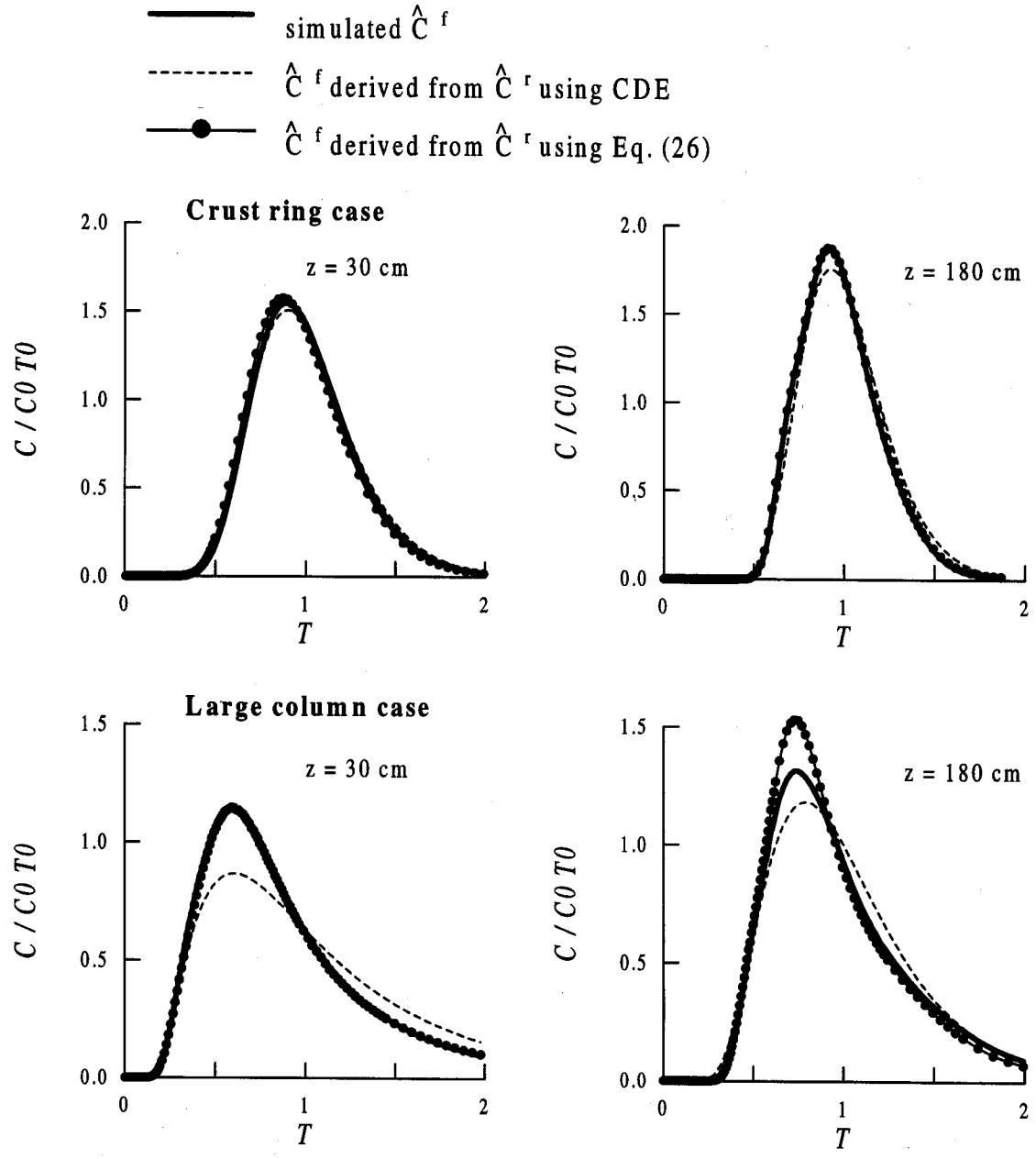

Fig. 8. *Simulated breakthrough curves of flux averaged concentrations, $\hat{C}^f$, and breakthrough curves of $\hat{C}^f$ derived from resident concentrations, $\hat{C}^r$, using (i) a 1-D CDE model, and (ii) Eqn. (26) assuming stochastic-convective solute transport.*

have lower peak concentrations and overestimate concentrations at later times especially for larger flow heterogeneity. Using Eqn. (26), the solute peak arrival times and the raising and falling limbs of the BTCs are well predicted but, at greater depths for the Kopecky ring and large column cases, peak concentrations are overestimated. The following criterion was used to evaluate the different prediction cases of $\hat{C}^f$:

$$IAE = \frac{\int_0^\infty | \hat{C}_s^f(t) - \hat{C}_p^f(t) | \, dt}{\int_0^\infty \hat{C}_s^f(t) dt} 100 \qquad (27)$$

with $\hat{C}_s^f$ and $\hat{C}_p^f$ the simulated and predicted flux concentrations, respectively, and *IAE* the integrated absolute error which represents the ratio of the area between the predicted and simulated BTC relative to the area of the simulated BTC. Figure 9 shows *IAE* calculated at different depths for the crust ring, Kopecky ring, and large column cases. Except for the crust ring case at shallower depths, Eqn. (26) predicts the simulated $\hat{C}^f$ equally well as the 1-D CDE which is calibrated to simulated $\hat{C}^f$ BTCs. At depths where solute transport can be conceptualised as a stochastic-convective process (λ_{eff} increases with travel distance, Fig. 6), Eqn. (26) gives better results to derive $\hat{C}^f$ from $\hat{C}^r$ than a 1-D CDE calibrated to $\hat{C}^r$ BTCs (Fig. 9).

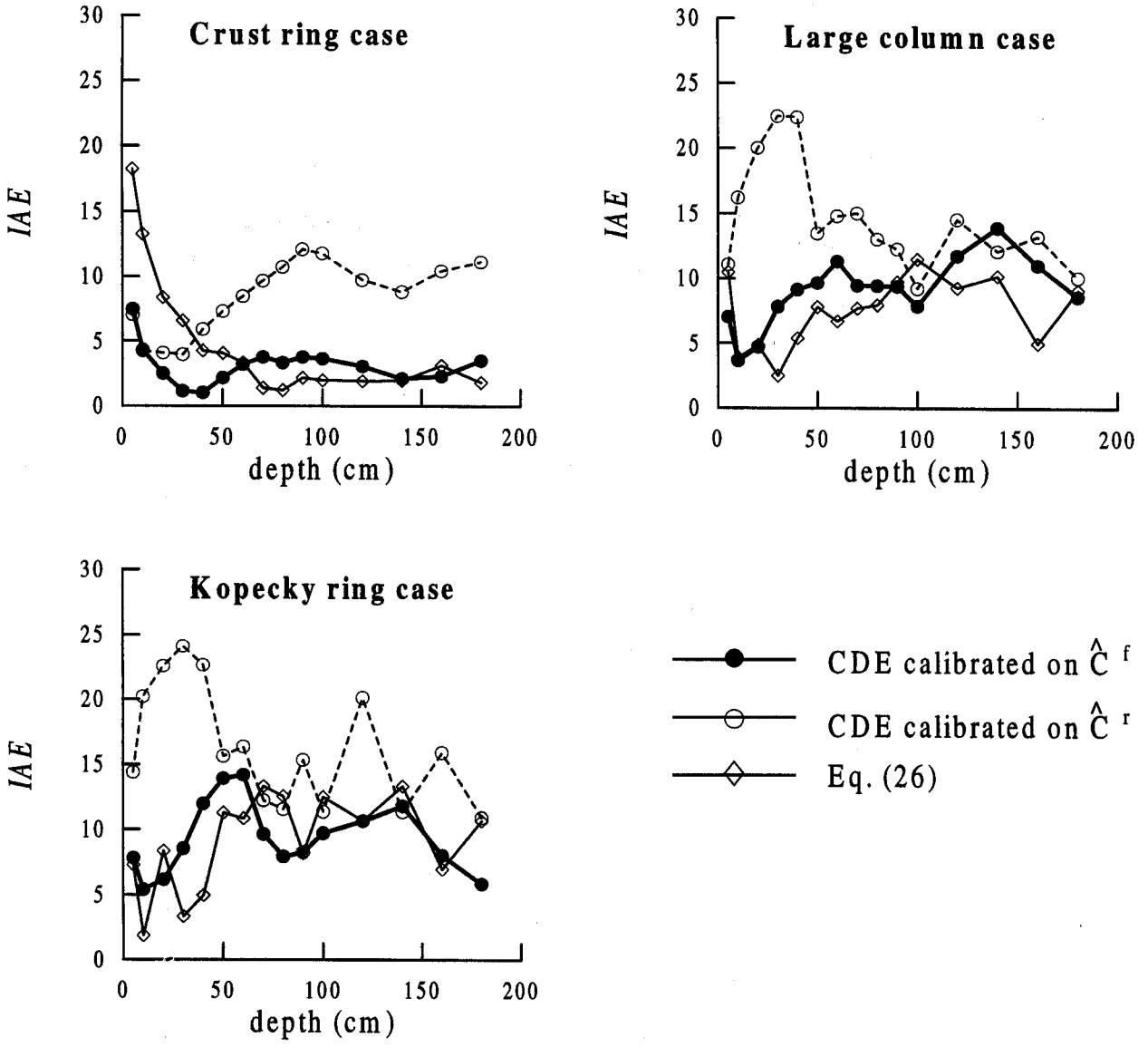

Fig. 9. *Integrated absolute error, IAE, between simulated breakthrough curves of field-scale flux averaged concentrations, $\hat{C}^f$, and breakthrough curves of $\hat{C}^f$ predicted by (i) a 1-D CDE calibrated to breakthrough curves of $\hat{C}^f$, (ii) a 1-D CDE calibrated to breakthrough curves of field-scale resident concentrations, $\hat{C}^r$, and (iii) by Eqn. (26) assuming stochastic-convective solute transport.*

At depths where the increase of λ_{eff} with travel distance is less significant, both derivation methods perform equally well. When $\hat{C}^r$ BTCs are described by the 1-D CDE in equivalent homogeneous soil columns (Eqn. (20)) with λ_{eff} and v_{eff} depending on the depth at which the $\hat{C}^r$ BTCs are described, evaluation of the mass balance equation (Eqn. (23b)) yields the following relation between $\hat{C}^f$ and $\hat{C}^r$:

$$\hat{C}^f = -\frac{\langle\theta\rangle}{\langle J_{w2}\rangle}\left[\begin{array}{l}\lambda_{eff}v_{eff}\dfrac{\delta\hat{C}^r}{\delta z} - v_{eff}\hat{C}^r \\ +\displaystyle\int_0^z\left(v_{eff}\frac{\delta\lambda_{eff}}{\delta z}+\lambda_{eff}\frac{\delta v_{eff}}{\delta z}\right)\frac{\delta\hat{C}^r}{\delta z} - \frac{\delta v_{eff}}{\delta z}\hat{C}^r dz\end{array}\right] \quad (28)$$

The integral in Eqn. (28) is neglected when $\hat{C}^f$ is predicted by a 1-D CDE model calibrated to a $\hat{C}^r$ BTC (Eqn. 24). Therefore, the differences between predictions of $\hat{C}^f$ by the 1-D CDE calibrated to $\hat{C}^r$ BTCs and simulated $\hat{C}^f$ result from the scale dependence of λ_{eff} and v_{eff} which is much more significant for heterogeneous media near the inlet surface where solute transport can be conceptualised as a stochastic-convective process. Deeper in the soil profile, where the stochastic-convective process shifts to a convective-dispersive process, the scale dependence of λ_{eff} and v_{eff} vanishes and the integral in Eqn. (28) can be neglected so that $\hat{C}^f$ can be derived from $\hat{C}^r$ BTC using a 1-D CDE.

Summary and Conclusions

For unsaturated flow conditions, observed field-scale solute dispersion in the macroporous loam profile considered could be predicted from the heterogeneity of macroscopic hydraulic properties using flow and transport simulations in generated heterogeneous profiles. To characterise the heterogeneity of the macroscopic hydraulic properties, the hydraulic conductivity curve, $K(h)$, should be measured on sufficiently small soil volumes. Since these $K(h)$ curves as well as the observed transport (cfr. Jacques *et al.*, 1997c) varied over a small scale, a dense sampling grid is required to characterise the spatial correlation of the hydraulic properties. Using the variability of the WRC or the pore size distribution to derive the variability of $K(h)$ indirectly based on the similar medium assumption led to considerable underestimation of solute flow heterogeneity and field-scale dispersivity. If small scale variations of the hydraulic conductivity are averaged out due to conductivity measurements having been made on larger samples (20cm I.D. 20cm long), field-scale solute dispersion was underestimated. Due to macroporosity, the variability of $K(h)$ derived from K_{sat}, measurements on small soil samples (5cm I.D, 5.1cm long), was much larger than the measured variability of $K(h)$ and the field-scale solute dispersion was overestimated when these K_{sat} measurements were used to characterise the heterogeneity of the hydraulic property.

For saturated flow conditions, solute transport heterogeneity at a smaller scale due to water flow and solute transport in different pore networks (macro- and micropore networks) should be considered. The water fluxes in the different pore networks and, hence, the solute transport heterogeneity and solute dispersion cannot be derived directly from K_{sat} or flux measurements in soil samples which represent the total flux, averaged over all networks.

The differences between field-scale flux and volume averaged concentrations are more significant for larger solute flow heterogeneity. When solute transport can be conceptualised as a stochastic-convective process, time series of flux-averaged concentrations predicted using a 1-D CDE calibrated to resident concentration BTCs overestimate the average solute arrival time and underestimate the peak concentrations. Using the relation between resident and flux concentrations for a stochastic-convective transport process gives better predictions of flux concentration BTCs derived from resident concentration BTCs.

Acknowledgements

The authors would like to thank the Belgian National Fund for Scientific Research (N.F.W.O.). The first author is a research assistant of the Belgian National Fund for Scientific Research (N.F.W.O.).

References

Ababou R., McLaughlin, D., Gelhar, L.W., and Tompson, A.B.F. 1989. Numerical simulation of three-dimensional saturated flow in randomly heterogeneous porous media. *Transp. Porous Media* 4:549–565.

Bear, J., 1972. *Dynamics of fluids in porous media*. Elsevier, New York.

Beven, K.J, Henderson, D.E., and Reeves, A.D. 1993. Dispersion parameters for undisturbed partially saturated soil. *J. Hydrol.* **143**: 19–43.

Bouma J. 1991. Influence of soil macroporosity on environmental quality. *Adv. Agron.* **46**: 1–37.

Cvetkovic, V., A.M. Shapiro, and G. Dagan, 1992. A solute flux approach to transport in heterogeneous formations. 2. Uncertainty analysis. *Wat. Resour. Res.* **28**: 1377–1388.

Dagan, G. 1989. *Flow and transport in porous formations*. Springer Verlag, New York.

Dagan, G., Cvetkovic, V., and Shapiro, A. 1992. A solute flux approach to transport in heterogeneous formations. 1. The general framework. *Wat. Resour. Res.* **28**: 1369–1376.

FAO, 1990. *FAO-Unesco soil map of the world. Revised legend.* Soils Bulletin 60. FAO, Rome. 119 pp.

Gelhar, L.W. 1993. *Stochastic subsurface hydrology*. Prentice Hall, Englewood Cliffs, NJ.

Gerke H.H., and van Genuchten, M.Th. 1993. A dual-porosity model for simulating the preferential movement of water and solutes in structured porous media. *Wat. Resour. Res.* **29**: 305–319.

Gutjahr, A. L., Hatch, S., and Bullard, B. 1995. *Random field generation, Conditional simulation, and flow modelling using the fast Fourier transform.* N.M. Inst. of Min. and Technol., Socorro, NM, USA.

Harter, T., and Yeh, T.-C. J. 1993. An efficient method for simulating steady unsaturated flow in random porous media: Using an analytical perturbation solution as initial guess to a numerical model. *Wat. Resour. Res.* **29**: 4139–4149.

Heimovaara, T.J., Focke, A.G., Bouten, W. and Verstraten, J.M. 1995. Assessing temporal variations in soil water composition with Time Domain Reflectometry. *Soil Sci. Soc. Am. J.* **59**: 689–698.

Hopmans, J., 1987. A comparison of various methods to scale soil hydraulic properties. *J. Hydrol.* **93**: 241–256.

Indelman P., and Dagan, G. 1993. Upscaling of conductivity of heterogeneous formations: general approach and application to isotropic media. *Transp. Porous Media* **12**: 161–183.

Jacques, D., Kim, D.-J., Diels, J., Vereecken, H., and Feyen, J. 1997a. Analysis of steady state chloride transport through two heterogeneous soils. *Wat. Resour. Res.* (Submitted)

Jacques, D., Vanderborght, J., Mallants, D., Mohanty, B.P., and Feyen, J 1997b. Analysis of solute redistribtution in heterogeneous soil: I Geostatistical approach. *Proceedings of the First European Conference on Geostatistics for Environmental Applications*, 20–22 November 1996, Lisbon, Portugal.

Jacques D., Vanderborght, J., Mallants, D., Kim, D.-J., Vereecken, H., and Feyen, J. 1997c. Evaluation of three stream tube models predicting field-scale solute transport. (In press.)

Jarvis, N.J., Jansson, P-E., Dik, P.E., and Messing, I. 1991. Modeling water and solute transport in macroporous soil. I. Model description and sensitivity analysis. *J. Soil Sci.* **42**: 59–70.

Jury, W.A. 1982. Simulation of solute transport using a transfer function model. *Wat. Resour. Res.* 18: 363–368.

Jury, W.A., 1985. *Spatial variability of soil physical parameters in solute migration: A critical literature review.* EPRI EA–4228 Project 2485–6, Riverside, CA.

Jury, W.A, and Roth, K. 1990. *Transfer functions and solute movement through soil: theory and applications.* Birkhäuser Verlag, Basel, Switzerland.

Jury, W.A., and Sposito, G. 1985. Field calibration and validation of solute transport models for the unsaturated zone. Soil *Sci. Soc. Am. J.* **49**: 1331–1341.

Kreft, A., and Zuber, A. 1978. On the physical meaning of the dispersion equation and its solution for different initial boundary conditions. *Chem. Engng. Sci.* **33**: 1471–1480.

Lauren, J.G., Wagenet, R.J., Bouma, J., and Wösten, J.H.M. 1988. Variability of saturated hydraulic conductivity in a glossudalfic hapludalf with macropores. *Soil Sci.*, **145**: 20–28.

Mallants D. 1996. *Water flow and solute transport in a heterogeneous soil profile.* Ph.D. dissertation, Katholieke Universiteit Leuven, Belgium.

Mallants, D., Mohanty, B.P., Jacques, D., and Feyen, J. 1996. Spatial variability of hydraulic properties in a multi-layered soil profile. *Soil Sci.*, **161**: 167–181.

Mallants, D., Mohanty, B.P., Vervoort, A. and Feyen, J. 1997a. Spatial analysis of the saturated conductivity of a soil with macropores. *Soil Technol.* 10: 115–131.

Mallants, D., Jacques, D., Tseng, P.-H., van Genuchten, M.Th., and Feyen, J. 1997b. Comparison of hydraulic property measurement methods using three sizes of soil cores. *J. Hydrol.* (in press)

Miller, E.E., and Miller, R.D. 1956. Physical theory for capillary flow phenomena. *J. Appl. Phys.* **27**: 324–332.

Mohanty, B.P., Kanwar, R.S., and Everts, C.J. 1994. Comparison of saturated conductivity measurement methods for a glacial till soil. *Soil Sci. Soc. Am. J.* **58**: 672–677.

Mualem, Y., 1976. A new model for predicting the hydraulic conductivity of unsaturated porous media. *Wat. Resour. Res.* **12**: 513–522.

Parker, J.C., and van Genuchten, M.Th. 1984. Flux-averaged and volume-averaged concentrations in continuum approaches to solute transport. *Wat. Resour. Res.* **20**: 866–872.

Richards, L.A., 1931. Capillary conduction of liquids through porous media. *Physics*, 1: 318–333.

Robin, M.J.L., Gutjahr, A.L., Sudicky, E.A., and Wilson, J.L. 1993. Cross-correlated random field generation with the direct Fourier transform method. *Wat. Resour. Res.* **29**: 2385–2397.

Rockhold, M.L., Rossi, R.E., and Hills, R.G. 1996. Application of similar media scaling and conditional simulation for modelling water flow and tritium transport at the Las Cruces Trench Site. *Wat. Resour. Res.* **32**: 595–609.

Russo, D., 1995a. On the velocity covariance and transport modeling in heterogeneous anisotropic porous formations. 1. Saturated flow. *Wat. Resour. Res.*, **31**: 129–137

Russo, D., 1995b. On the velocity covariance and transport modeling in heterogeneous anisotropic porous formations. 2. Unsaturated flow. *Wat. Resour. Res.*, **31**: 139–145.

Russo, D., and Bouton, M. 1992. Statistical analysis of spatial variability in unsaturated flow parameters. *Wat. Resour. Res.*, **28**: 1911–1925.

Shapiro, A.M., and Cvetkovic, V.D. 1988. Stochastic analysis of solute arrival time in heterogeneous porous media. *Wat. Resour. Res.*, **24**: 1711–1718.

Šimůnek, J., Vogel, T., and van Genuchten, M.Th. 1994. *The SWMS_2D code for simulating water flow and solute transport in two-dimensional variably saturated media.* Research Report No. 132, U.S. Salinity Lab., ARS, USDA, Riverside, CA, USA.

Simmons, C.S, 1982. A stochastic-convective transport representation of dispersion in one-dimensional porous media systems. *Wat. Resour. Res.* **18**: 1193–1214.

Soil Survey Staff, 1992. *Keys to soil taxonomy*, Sixth Edition, 1994.

Sposito, G., and Barry, D.A. 1987. On the Dagan model of solute transport in groundwater: foundational aspects. *Wat. Resour. Res.* **23**: 1867–1875.

Tompkins, J.A., Gan, K.C., Wheater, H.S., and Hirano, F. 1994. Prediction of solute dispersion in heterogeneous porous media: effects of ergodicity and hydraulic conductivity discretisation. *J. Hydrol.*, **159**: 105–123.

Toride, N., and Leij, F.J. 1996. Convective-dispersive stream tube model for field-scale solute transport: I Moment analysis. *Soil Sci. Soc. Am. J.* **60**:352–361.

Tseng, P.-H., and Jury, W. 1994. Comparison of transfer function and deterministic modeling of area-averaged solute transport in a heterogeneous field. *Wat. Resour. Res.* **30**: 2051–2063.

van Genuchten, M.Th., 1980. A closed form equation for predicting the hydraulic conductivity of unsaturated soils. *Soil Sci. Soc. Am. J.* **44**: 892–898.

van Wesenbeeck, I.J., and Kachanoski, R.G. 1995. Predicting field-scale solute transport using in-situ measurements of soil hydraulic properties. *Soil Sci. Soc. Am. J.* **59**:734–742.

Vogel. T, Cislerova, M., and Hopmans, J.W. 1991. Porous media

with linearly variable hydraulic properties. *Wat. Resour. Res.* 27: 2735–2741.

Warrick, A.W., Mullen, G.J., and Nielsen, D.R. 1977. Scaling field-measured soil hydraulic properties using a similar media concept. *Wat. Resour. Res.* 13: 355–362.

White, R.E., 1985. The influence of macropores on the transport of dissolved and suspended matter through soil. *Adv. Soil Sci.* 3: 95–121.

Yeh, T.-C. J., Gelhar, L.W., and Gutjahr, A.L. 1985a. Stochastic analysis of unsaturated flow in heterogeneous soils. 1. Statistically isotropic media. *Wat. Resour. Res.*, 21: 447–456.

Yeh, T.-C. J., Gelhar, L.W., and Gutjahr, A.L. 1985b. Stochastic analysis of unsaturated flow in heterogeneous soils. 2. Statistically anisotropic media with variable a. *Wat. Resour. Res.*, 21: 457–464.